PHYSICAL REVIEW D **87,** 025003 (2013)

Sensitivities of the IceCube DeepCore detector to signatures of low-mass dark matter in the Galactic halo

Fei-Fan Lee,[1] Guey-Lin Lin,[1] and Yue-Lin Sming Tsai[2,3]

[1]*Institute of Physics, National Chiao-Tung University, Hsinchu 30010, Taiwan*
[2]*National Centre for Nuclear Research, Hoża 69, 00-681 Warsaw, Poland*
[3]*Kavli Institute for Theoretical Physics, CAS, Beijing 100190, China*

(Received 17 October 2012; published 2 January 2013)

We discuss the event rate in the DeepCore array due to neutrino flux produced by annihilations and decays of Galactic dark matter. This event rate is calculated with a 10 GeV threshold energy, which is smaller than the threshold energy taken in previous works. Taking into account the background event rate due to the atmospheric neutrino flux, we evaluate the sensitivity of the DeepCore array for probing the dark matter annihilation cross section and decay time. The sensitivity studies include the annihilation modes $\chi\chi \to b\bar{b}$, $\tau^+\tau^-$, $\mu^+\mu^-$, and $\nu\bar{\nu}$, and decay modes $\chi \to b\bar{b}$, $\tau^+\tau^-$, $\mu^+\mu^-$, and $\nu\bar{\nu}$. We compare our results with corresponding constraints derived from observations of WMAP, ACT, and Fermi-LAT.

DOI: 10.1103/PhysRevD.87.025003 PACS numbers: 14.60.Pq, 14.60.St

I. INTRODUCTION

Many astrophysical observations indicate the existence of dark matter (DM). A good example of such observations is the measurement of rotation curves for stars and gas in spiral galaxies. On the other hand, the nature of DM remains to be unveiled. In this regard, many DM candidates have been proposed with the proposal of weak interacting massive particles (WIMPs) [1,2] the most popular among all candidates. The detections of DM shall test the idea of WIMPs. The detections of DM can be categorized into direct and indirect approaches. The former approach proceeds by observing the nucleus recoil as DM interacts with the target nuclei in the detector. The latter approach relies on detecting final state particles resulting from DM annihilations or decays. In this article, we focus on the indirect detection of DM through observing neutrinos produced by DM annihilations or decays in the Galactic halo.

The search for neutrinos coming from DM annihilations in the Galactic halo has been performed by IceCube [3]. Data obtained from the IceCube 22-string configuration set the 90% C.L. upper limit on DM annihilation cross section $\langle\sigma v\rangle \sim 10^{-22}$ cm^3 s^{-1} for the $\chi\chi \to \nu\bar{\nu}$ channel at $m_\chi =$ 1 TeV [4], while the preliminary result of the IceCube 40-string Galactic-center analysis improves the above limit to 10^{-23} cm^3 s^{-1} [5]. Based upon the IceCube 40-string data selection for searching diffuse flux of astrophysical muon neutrinos [6], a comparable constraint on the cross section of $\chi\chi \to \nu\bar{\nu}$ annihilations, which could take place in the core of Earth, is derived [7] for TeV range dark-matter masses. Furthermore, upper limits on the annihilation cross sections of $\chi\chi \to \mu^+\mu^-$ and $\chi\chi \to \tau^+\tau^-$ channels are also obtained. It is interesting to compare these upper limits with the required annihilation cross sections for the same channels for explaining the PAMELA data on positron fraction excess [8] and Fermi large area telescope (Fermi-LAT) $e^+ + e^-$ fluxes measurement [9]. As shown in Ref. [4], the IceCube upper limit on the $\chi\chi \to \tau^+\tau^-$ annihilation cross section is comparable to the required $\chi\chi \to \tau^+\tau^-$ annihilation cross section for explaining PAMELA and Fermi-LAT data. On the other hand, the IceCube upper limit on the $\chi\chi \to \mu^+\mu^-$ annihilation cross section is still too high to test the idea of using this mode to account for PAMELA and Fermi-LAT data.

The IceCube sensitivity on the DM search is expected to improve with the data from all 86 strings analyzed. The analysis of DeepCore array data will further enhance the sensitivity. The DeepCore array [10–12] is located in the deep center region of the IceCube detector. This array consists of eight densely instrumented strings plus the nearest standard IceCube strings. The installation of the DeepCore array significantly improves the rejection of downward going atmospheric muons in IceCube and lowers the threshold energy for detecting muon track or cascade events to about 5 GeV. This muon rejection is crucial for IceCube to observe the DM-induced neutrino signature from the Galactic halo. In fact, it has been pointed out that the parameter range for the $\chi\chi \to \mu^+\mu^-$ channel preferred by PAMELA and Fermi-LAT data could be stringently constrained [13–15] (see also discussions in Ref. [16]) by the data from the IceCube detector augmented with the DeepCore array. In this work, we shall, however, focus on the low-mass DM instead of DM with its mass in the range preferred by PAMELA and Fermi-LAT.

We note that previous analyses on DeepCore sensitivity [15,17] have set the threshold energy at (40–50) GeV for both track and cascade events. However, to take full advantage of the DeepCore array, it is desirable to include neutrino events in the energy range 10 GeV $\leq E_\nu \leq$ 50 GeV. We have initiated such a study for track events [18]. In this work, we generalize the previous study to cascade events in the IceCube DeepCore detector. Since we are only interested in low-mass DM, we only consider

channels $\chi\chi \to b\bar{b}$, $\tau^+\tau^-$, $\mu^+\mu^-$, and $\nu\bar{\nu}$ for annihilations and channels $\chi \to b\bar{b}$, $\tau^+\tau^-$, $\mu^+\mu^-$, and $\nu\bar{\nu}$ for decays. The neutrino fluxes generated through DM annihilations or decays into $t\bar{t}$, W^+W^-, and ZZ final states are not included in this analysis.

This paper is organized as follows. In Sec. II we describe neutrino fluxes from DM annihilation or decay at the Galactic halo for different halo profiles. In Sec. III we briefly describe our results on the background atmospheric neutrino fluxes, taking into account neutrino oscillations. In Sec. IV we present our results on the projected five year sensitivity of the DeepCore array on cascade events induced by DM annihilations and decays. In addition, we also compare our results with the up-to-date indirect detection limits from Fermi-LAT gamma-ray data and cosmic microwave background (CMB) observations. Specifically, we shall compare the DeepCore sensitivities on DM annihilation cross section $\langle\sigma v\rangle$ and DM decay time with corresponding constraints obtained from gamma-ray observations [19,20] (see also analysis in Ref. [21]) and those obtained from CMB anisotropy [22,23] based on one or both of the recent WMAP 7-year [24] and ACT 2008 [25] data. Discussions and conclusions are given in Sec. V.

II. NEUTRINO FLUX FROM ANNIHILATIONS AND DECAYS OF DARK MATTER IN THE GALACTIC HALO

The differential neutrino flux from the Galactic dark matter halo for neutrino flavor i can be written as [26]

$$\frac{d\Phi_{\nu_i}}{dE_{\nu_i}} = \frac{\Delta\Omega}{4\pi}\frac{\langle\sigma v\rangle}{2m_\chi^2}\left(\sum_F B_F \frac{dN_{\nu_i}^F}{dE}\right) R_\odot \rho_\odot^2 \times J_2(\Delta\Omega) \quad (1)$$

for the case of annihilating DM, and

$$\frac{d\Phi_{\nu_i}}{dE_{\nu_i}} = \frac{\Delta\Omega}{4\pi}\frac{1}{m_\chi \tau_\chi}\left(\sum_F B_F \frac{dN_{\nu_i}^F}{dE}\right) R_\odot \rho_\odot \times J_1(\Delta\Omega) \quad (2)$$

for the case of decaying DM, where $R_\odot = 8.5$ kpc is the distance from the Galactic center (GC) to the solar system, $\rho_\odot = 0.3$ GeV/cm^3 is the DM density in the solar neighborhood, m_χ is the DM mass, τ_χ is the DM decay time, and $dN_{\nu_i}^F/dE$ is the neutrino spectrum per annihilation or decay for a given annihilation or decay channel F with a corresponding branching fraction B_F. For the $\chi\chi \to \nu\bar{\nu}$ channel, we assume that two neutrinos are produced per annihilated DM pair and all neutrino flavors are equally populated. Thus the neutrino spectrum per flavor is a monochromatic line with $dN_\nu/dE = \frac{2}{3}\delta(E - m_\chi)$. On the other hand, the neutrino spectrum per flavor for the $\chi \to \nu\bar{\nu}$ channel is $dN_\nu/dE = \frac{2}{3}\delta(E - \frac{m_\chi}{2})$. The neutrino spectra $dN_{\nu_i}^F/dE$ for other channels are summarized in Refs. [17,27]. The quantity $\langle\sigma v\rangle$ is the thermally averaged annihilation cross section, which can be written as

$$\langle\sigma v\rangle = B\langle\sigma v\rangle_0, \quad (3)$$

with a boost factor B [28]. We set $\langle\sigma v\rangle_0 = 3\times10^{-26}$ cm^3 s^{-1}, which is the typical annihilation cross section for the present dark matter abundance under the standard thermal relic scenario [1]. We treat the boost factor B as a phenomenological parameter. The dimensionless quantity $J_n(\Delta\Omega)$ is the DM distribution integrated over the line of sight (l.o.s) and averaged over a solid angle $\Delta\Omega = 2\pi(1 - \cos\psi_{\max})$, i.e.,

$$J_n(\Delta\Omega) = \frac{1}{\Delta\Omega}\int_{\Delta\Omega} d\Omega \int_{\text{l.o.s}} \frac{dl}{R_\odot}\left(\frac{\rho(r(l,\psi))}{\rho_\odot}\right)^n, \quad (4)$$

where ρ is the DM density at a specific location described by the coordinate (l, ψ) with l the distance from the Earth to DM and ψ the direction of DM viewed from the Earth with $\psi = 0$ corresponding to the direction of GC. The distance $r \equiv \sqrt{R_\odot^2 + l^2 - 2R_\odot l\cos\psi}$ is the distance from GC to DM. We note that the above definition of J_n includes the constant factors $\Delta\Omega$, $R_\odot$, and $\rho_\odot$ in the denominator. This definition differs from that adopted in papers by IceCube and Fermi-LAT collaborations (see, for example, Refs. [4,20]) where the above-mentioned constant factors are not included. We computed the values of $J_n(\Delta\Omega)$ with DarkSUSY [29]. For the Galactic DM distribution, we consider Navarro-Frenk-White (NFW) [30], Einasto [31–33], and Isothermal profiles [34]. The functional forms of these profiles are given by

$$\rho_{\text{NFW}}(r) = \rho_s \frac{R_s}{r}\left(1 + \frac{r}{R_s}\right)^{-2}, \quad (5)$$

$$\rho_{\text{Ein}}(r) = \rho_s \times \exp\left\{-\frac{2}{\alpha}\left[\left(\frac{r}{R_s}\right)^\alpha - 1\right]\right\}, \quad \alpha = 0.17, \quad (6)$$

$$\rho_{\text{Iso}}(r) = \frac{\rho_s}{1 + (r/R_s)^2}, \quad (7)$$

with values of R_s and ρ_s given in Table I. In all cases we impose the normalization $\rho_\odot = 0.3$ GeV/cm^3, which is at $r = 8.5$ kpc. The comparison of different DM halo models is shown in Fig. 1.

Neutrinos are significantly mixed through oscillations when they travel a vast distance across the galaxy. The observed flavor ratio of DM-induced neutrinos is related to the flavor ratio at the source through the probability matrix $P_{\alpha\beta} \equiv P(\nu_\beta \to \nu_\alpha)$ [35–37]. In particular, the exact form of $P_{\alpha\beta}$ in terms of mixing angles θ_{ij} and CP phase δ is given in Ref. [37]. The mixing angles θ_{23} and θ_{12} have been well measured while the newest results for θ_{13} from

TABLE I. Parameters of the density profiles for the DM halo.

DM halo model	R_s (kpc)	ρ_s (GeV/cm^3)
NFW	20.0	0.260
Einasto	21.5	0.0538
Isothermal	3.50	2.07

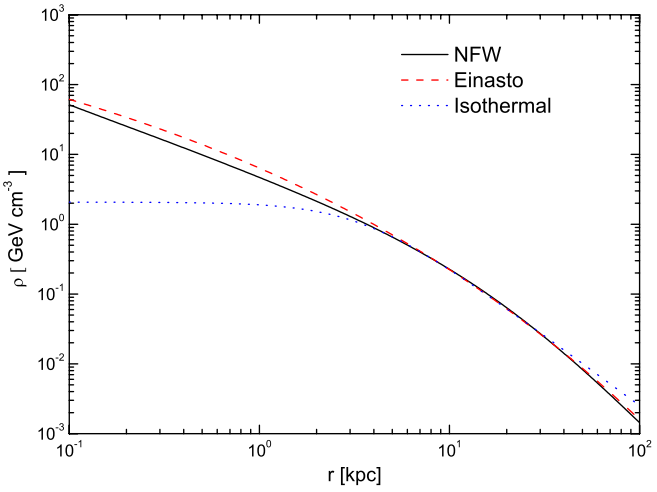

FIG. 1 (color online). Comparison of the dark matter density distribution, $\rho(r)$, as a function of distance from the Galactic center as described by the NFW, Einasto, and Isothermal halo models.

accelerator [38] and reactor experiments [39–41] are also available. We take $\sin^2\theta_{23} = 0.386$, $\sin^2\theta_{12} = 0.307$, $\sin^2\theta_{13} = 0.0241$, and $\delta = 1.08\pi$, which are best fit values of neutrino mixing parameters from a recent global fitting [42] in the case of normal mass hierarchy. Therefore,

$$\begin{aligned}\Phi_{\nu_e} &= 0.55\Phi^0_{\nu_e} + 0.24\Phi^0_{\nu_\mu} + 0.21\Phi^0_{\nu_\tau},\\ \Phi_{\nu_\mu} &= 0.24\Phi^0_{\nu_e} + 0.40\Phi^0_{\nu_\mu} + 0.35\Phi^0_{\nu_\tau},\\ \Phi_{\nu_\tau} &= 0.21\Phi^0_{\nu_e} + 0.35\Phi^0_{\nu_\mu} + 0.44\Phi^0_{\nu_\tau},\end{aligned} \tag{8}$$

where $\Phi^0_{\nu_i}$ and $\Phi_{\nu_{\nu_i}}$ are neutrino fluxes at the source and on the earth, respectively. While the best fit neutrino mixing parameters differ slightly in the case of inverted mass hierarchy, they do not produce noticeable change in the above relation.

III. ATMOSPHERIC NEUTRINO FLUXES

We follow the approaches in Refs. [18,43,44] to compute the intrinsic atmospheric neutrino background fluxes. The ν_μ flux arising from π decays reads

$$\begin{aligned}\frac{\mathrm{d}^2N^\pi_{\nu_\mu}(E,\xi,X)}{\mathrm{d}E\mathrm{d}X} &= \int_E^\infty \mathrm{d}E_N \int_E^{E_N} \mathrm{d}E_\pi \frac{\Theta(E_\pi - \frac{E}{1-\gamma_\pi})}{d_\pi E_\pi(1-\gamma_\pi)}\\ &\times \int_0^X \frac{\mathrm{d}X'}{\lambda_N} P_\pi(E_\pi, X, X')\frac{1}{E_\pi}F_{N\pi}(E_\pi, E_N)\\ &\times \exp\left(-\frac{X'}{\Lambda_N}\right)\phi_N(E_N),\end{aligned} \tag{9}$$

where E is the neutrino energy, X is the slant depth in units of gram per square centimeter, ξ is the zenith angle in the direction of incident cosmic-ray nucleons, $r_\pi = m^2_\mu/m^2_\pi$, d_π is the pion decay length in units of gram per square centimeter, λ_N is the nucleon interaction length while Λ_N is the corresponding nucleon attenuation length, and $\phi_N(E_N)$ is the primary cosmic-ray spectrum. We have $\phi_N(E_N) = \sum_A A\phi_A(E_N)$ with A the atomic number of each nucleus. The spectrum of each cosmic-ray component is parametrized by [45,46]

$$\phi_A(E_N) = K \times (E_N + b\exp[-c\sqrt{E_N}])^{-\alpha}, \tag{10}$$

in units of per square meter per second per steradian per GeV. The fitting parameters α, K, b, c depend on the type of nucleus. They are tabulated in Ref. [46]. The function $P_\pi(E_\pi, X, X')$ is the probability that a charged pion produced at the slant depth X' survives to the depth $X(>X')$ [47]. $F_{N\pi}(E_\pi, E_N)$ is the normalized inclusive cross section for $N + \text{air} \to \pi^\pm + Y$ and is given in Ref. [43]. The kaon contribution to the atmospheric ν_μ flux has the same form as Eq. (9) with an inclusion of the branching ratio $B(K \to \mu\nu) = 0.635$ and appropriate replacements in kinematic factors as well as in the normalized inclusive cross section. The three-body muon decay contribution to the atmospheric ν_μ flux is also included. The details are discussed in Ref. [44]. After summing the two-body and three-body decay contributions, we obtain the total intrinsic atmospheric muon neutrino flux. From Fig. 1 of Ref. [18], we note that the angle-averaged atmospheric muon neutrino flux obtained by our calculation and that obtained by Honda *et al.* [48] both agree well with AMANDA-II results [49].

The intrinsic atmospheric ν_τ flux due to D_s decays can be obtained by solving cascade equations [44,50]. One obtains

$$\frac{\mathrm{d}^2N_{\nu_\tau}(E,X)}{\mathrm{d}E\mathrm{d}X} = \frac{Z_{ND_s}Z_{D_s\nu_\tau}}{1-Z_{NN}} \cdot \frac{\exp(-X/\Lambda_N)\phi_N(E_N)}{\Lambda_N}, \tag{11}$$

where $Z_{NN} \equiv 1 - \lambda_N/\Lambda_N$, Z_{ND_s} and $Z_{D_s\nu_\tau}$ are the Z moments defined in our previous work [18]. Finally, the atmospheric ν_μ flux taking into account the neutrino oscillation effect is given by

$$\begin{aligned}\frac{\mathrm{d}\bar{N}_{\nu_\mu}(E,\xi)}{\mathrm{d}E} = \int \mathrm{d}X\Big[&\frac{\mathrm{d}^2N_{\nu_\tau}}{\mathrm{d}E\mathrm{d}X}\cdot P_{\nu_\tau\to\nu_\mu}\\ &+ \frac{\mathrm{d}^2N_{\nu_\mu}}{\mathrm{d}E\mathrm{d}X}\cdot(1 - P_{\nu_\mu\to\nu_\tau})\Big],\end{aligned} \tag{12}$$

where $P_{\nu_\alpha\to\nu_\beta}$ is the $\nu_\alpha \to \nu_\beta$ oscillation probability. Subleading contributions to atmospheric ν_μ flux arising from $\nu_\mu \to \nu_e$ and $\nu_e \to \nu_\mu$ oscillations are not included in the above equation. We can write down the atmospheric ν_τ flux in the similar way.

IV. RESULTS

In IceCube DeepCore, the track event rate for contained muons is given by

$$\begin{aligned}\Gamma_\mu = &\int_{E^{\mathrm{th}}_\mu}^{E_{\max}} \mathrm{d}E_\mu \int_{E_\mu}^{E_{\max}} \mathrm{d}E_{\nu_\mu} N_A \rho_{\mathrm{ice}} V_{\mathrm{tr}}\\ &\times \frac{d\Phi_{\nu_\mu}}{dE_{\nu_\mu}}\cdot\frac{d\sigma^{\mathrm{CC}}_{\nu N}(E_{\nu_\mu}, E_\mu)}{dE_\mu} + (\nu \to \bar{\nu}),\end{aligned} \tag{13}$$

while the cascade event rate is given by

$$\Gamma_{\rm casc} = \int_{E_{\rm sh}^{\rm th}}^{E_{\rm max}} {\rm d}E_{\rm sh} \int_{E_{\rm sh}}^{E_{\rm max}} {\rm d}E_\nu N_A \rho_{\rm ice} V_{\rm casc} \times \frac{d\Phi_\nu}{dE_\nu} \cdot \frac{d\sigma_{\nu N}(E_\nu, E_{\rm sh})}{dE_{\rm sh}} + (\nu \to \bar{\nu}), \quad (14)$$

where $\rho_{\rm ice} = 0.9\ {\rm g\,cm^{-3}}$ is the density of ice, $N_A = 6.022 \times 10^{23}\ {\rm g^{-1}}$ is Avogadro's number, $V_{\rm tr} \approx 0.04\ {\rm km^3}$ is the effective volume of the IceCube DeepCore array for muon track events [10,15] and $V_{\rm casc} \approx 0.02\ {\rm km^3}$ is that for cascade events [15,51], $d\Phi_\nu/dE_\nu$ is the neutrino flux arrived at IceCube, which is the sum of DM-induced flux and the background atmospheric neutrino flux, $E_{\rm max}$ is taken as m_χ for annihilation and $m_\chi/2$ for decay, $E_\mu^{\rm th}$ and $E_{\rm sh}^{\rm th}$ are the threshold energies for track events and cascade events, respectively, $d\sigma_{\nu N}^{\rm CC}/dE_\mu$ is the differential cross section of neutrino-nucleon charged-current scattering, and $d\sigma_{\nu N}/dE_{\rm sh}$ is the differential cross section for showers produced by neutrino-nucleon charged-current and neutral-current scatterings. In this work, we use differential cross sections $d\sigma_{\nu N}^{\rm CC}/dE_\mu$ and $d\sigma_{\nu N}/dE_{\rm sh}$ given by Ref. [52] with CTEQ6 parton distribution functions. The atmospheric part of $d\Phi_{\nu_e}/dE_{\nu_e}$ is taken from Ref. [48]. We also set $E_\mu^{\rm th} = E_{\rm sh}^{\rm th} = 10$ GeV. It should be noted that the value for $V_{\rm tr}$ is an average effective volume based on the energy dependent $V_{\rm tr}$ discussed in Ref. [10], while the value for $V_{\rm casc}$ is just the instrumental volume of the DeepCore detector. The updated effective volumes of the DeepCore detector for track and cascade events are available in Ref. [53]. While we adopt constant effective volumes for evaluating DeepCore sensitivities, we shall also estimate how much the updated effective volumes affect our results.

As mentioned earlier, we consider neutrino fluxes generated through the annihilation channels $\chi\chi \to b\bar{b}$, $\tau^+\tau^-$, $\mu^+\mu^-$, and $\nu\bar{\nu}$, and the decay channels $\chi \to b\bar{b}$, $\tau^+\tau^-$, $\mu^+\mu^-$, and $\nu\bar{\nu}$. By computing the cascade event rates, we present in Fig. 2 the required DM annihilation cross section as a function of m_χ such that the neutrino signature from DM annihilations can be detected at the 2σ significance in five years. The 2σ statistical significance is defined as

$$\frac{N_s}{\sqrt{N_s + N_b}} = 2, \quad (15)$$

where N_s and N_b are numbers of signal and background events, respectively. In Fig. 2, we take the NFW profile for DM density distribution in the Galactic halo, the shower threshold energy $E_{\rm sh}^{\rm th} = 10$ GeV, and the cone half-angle $\psi_{\rm max} = 50°$. Nondetection of the DM neutrino signature would then exclude the parameter region above the curve at the 2σ level. We have presented results corresponding to different annihilation channels. It is seen that the required annihilation cross section for the 2σ detection significance is smallest for the channel $\chi\chi \to \nu\bar{\nu}$ and largest for the channel $\chi\chi \to b\bar{b}$.

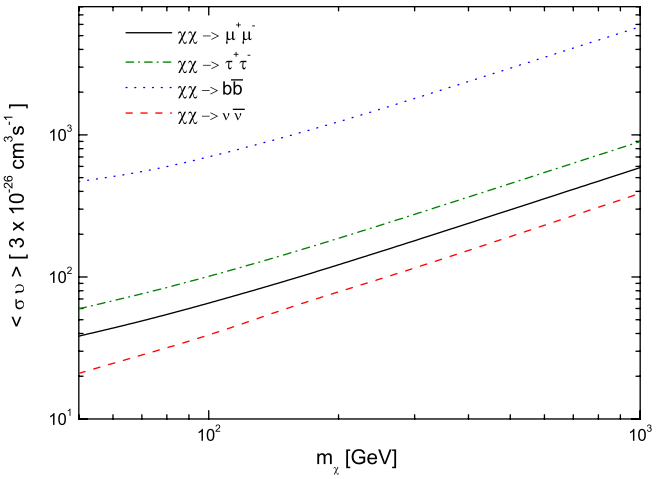

FIG. 2 (color online). The dotted line, dot-dashed line, solid line, and dashed line are the expected DeepCore sensitivities to DM annihilation cross section with the detection of cascade events from $\chi\chi \to b\bar{b}$, $\chi\chi \to \tau^+\tau^-$, $\chi\chi \to \mu^+\mu^-$, and $\chi\chi \to \nu\bar{\nu}$ channels, respectively. We adopt the NFW profile for obtaining the results in this figure and those in the subsequent figures except Fig. 4.

At this juncture, it is desirable to estimate effects of the updated effective volume on our sensitivity calculations. The energy dependent effective volume $V_{\rm casc}(E)$ as given in Ref. [53] is roughly 3 times smaller than the value $0.02\ {\rm km^3}$ adopted in our calculation for $E_\nu = 10$ GeV. On the other hand, $V_{\rm casc}(E)$ increases monotonically with energy with $V_{\rm casc}(E)$ greater than $0.02\ {\rm km^3}$ for $E_\nu > 40$ GeV. For the annihilation process $\chi\chi \to \nu\bar{\nu}$, one has $E_\nu = m_\chi$. Hence the DeepCore sensitivity to this process should be better than that presented in Fig. 2, which starts from $m_\chi = 50$ GeV. For the $\chi\chi \to \mu^+\mu^-$ mode, $m_\chi = 50$ GeV corresponds to $E_\nu \simeq 20$ GeV. At this energy, the value $V_{\rm casc} = 0.02\ {\rm km^3}$ overestimates the effective volume by about a factor of 2; thus the DeepCore sensitivity to $\langle\sigma(\chi\chi \to \mu^+\mu^-)v\rangle$ should be corrected by a factor of $\sqrt{2} \approx 1.4$. The correction factor gradually reduces to 1 as m_χ approaches about 120 GeV, which corresponds to $E_\nu = 40$ GeV. For $m_\chi > 120$ GeV, the DeepCore sensitivity calculated with $V_{\rm casc}(E)$ is better than that presented in Fig. 2. The correction factor for $\chi\chi \to \tau^+\tau^-$ is similar to that for $\chi\chi \to \mu^+\mu^-$. The hadronic mode $\chi\chi \to b\bar{b}$ requires a different correction factor for the same m_χ. However, we shall not address such a correction here since the DeepCore detector is relatively insensitive to $\chi\chi \to b\bar{b}$.

Next, we show how the DeepCore sensitivity on the DM annihilation cross section varies with the chosen cone half-angle and threshold energy for the NFW DM density profile. Here we take the $\chi\chi \to \mu^+\mu^-$ channel for illustration. Figure 3 shows the required DM annihilation cross section $\langle\sigma(\chi\chi \to \mu^+\mu^-)v\rangle$ for a 2σ detection in five years for different cone half-angle $\psi_{\rm max}$. It is seen that

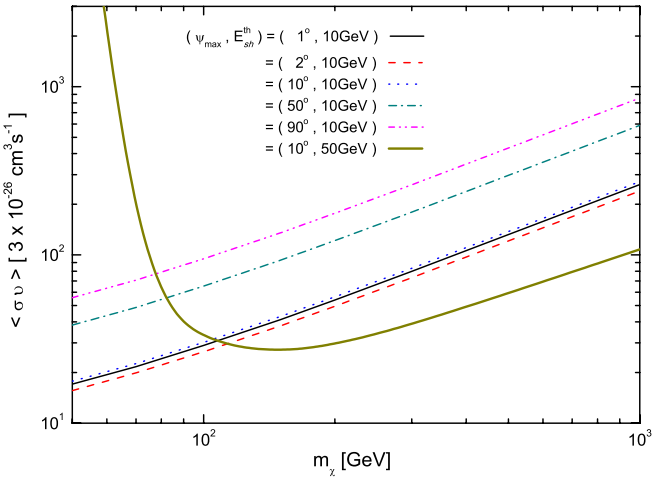

FIG. 3 (color online). The required DM annihilation cross section ($\chi\chi \to \mu^+\mu^-$) as a function of m_χ such that the cascade events induced by neutrinos from DM annihilations can be detected at the 2σ significance in five years. Results corresponding to different $\psi_{\max}$ are presented. For comparison, we also show the result with $E_{\rm sh}^{\rm th} = 50$ GeV and $\psi_{\max} = 10°$ [17].

the sensitivity is improved as $\psi_{\max}$ increases from 1° to 2° while it turns weaker as $\psi_{\max}$ increases further. In the latter case, the signal increases slower than the background does. We should point out that the choice of $\psi_{\max}$ depends on the angular resolution of the experiment. The current angular resolution in IceCube for cascade events is 50°. However, an improvement on such a resolution is expected [54]. In fact, a new reconstruction method that can achieve a 5° angular resolution for cascade events in large-scale neutrino telescopes has been proposed [55]. Hence results shown in Fig. 3 with $\psi_{\max} \geq 10°$ can be realized in the near future. In this figure, we also show the result for a higher threshold energy $E_{\rm sh}^{\rm th} = 50$ GeV with a cone half-angle $\psi_{\max} = 10°$ for comparison. This result is taken from Ref. [17] where $\psi_{\max} = 10°$ is identified as the most optimal cone half-angle for constraining the DM annihilation cross section at that threshold energy. For large m_χ, lowering $E_{\rm sh}^{\rm th}$ from 50 to 10 GeV does not affect much the signal rate, while it significantly increases the atmospheric background event rate. Hence, the sensitivity on the DM annihilation cross section becomes worse by choosing $E_{\rm sh}^{\rm th} = 10$ GeV. One expects that the situation turns opposite for m_χ approaching the threshold energy. In fact, for $m_\chi < 100$ GeV, one can see that the sensitivity on the DM annihilation cross section obtained with $E_{\rm sh}^{\rm th} = 10$ GeV is always better than that obtained with $E_{\rm sh}^{\rm th} = 50$ GeV. We note that the DeepCore sensitivities on other annihilation channels have similar cone half-angle and threshold energy dependencies. From the above discussions, we observe that, in contrast to the main concern of this article, raising the shower threshold energy gains sensitivity for probing heavier DM. In fact, as the threshold energy approaches 100 GeV, one enters into the operative energy range of the full IceCube array such that the effective volume of the detector increases more rapidly with the threshold energy than the case with the DeepCore detector alone [53]. The same situation holds for probing DM annihilation with track events.

After discussing how the DeepCore sensitivities on the DM annihilation cross section vary with the chosen cone half-angle and threshold energy for the NFW profile, we study the variation of DeepCore sensitivities on $\chi\chi \to \mu^+\mu^-$ with $\psi_{\max}$ for different DM density profiles. First, we present in Fig. 4 our expected DeepCore sensitivities corresponding to different $\psi_{\max}$ for the Einasto DM density profile. Similar to the NFW profile, the Einasto DM density distribution also has a cusp in the central DM region. We refer to this class of DM density profiles as the cusped profile. Therefore the DeepCore sensitivity on $\langle\sigma(\chi\chi \to \mu^+\mu^-)v\rangle$ with the Einasto profile becomes poorer as $\psi_{\max}$ increases. In addition, we can see from Fig. 1 that the DM density of the Einasto profile is higher than that of the NFW profile between 0.1 and 5 kpc from the GC, and both density profiles are almost identical beyond this range of distances. Hence the DeepCore sensitivity on $\langle\sigma(\chi\chi \to \mu^+\mu^-)v\rangle$ with the Einasto profile is better than that with the NFW profile for $\psi_{\max} = 50°$. Next, we also present in Fig. 4 the expected DeepCore sensitivities for different $\psi_{\max}$ with the isothermal DM density profile. Because there is a core in the central DM density distribution of the isothermal profile, we refer to this class of profile as the cored profile. We note that the sensitivity to the DM annihilation cross section with the isothermal profile improves as $\psi_{\max}$ increases from 1° to 50° while the sensitivity with the Einasto profile behaves oppositely. This is because the DM density

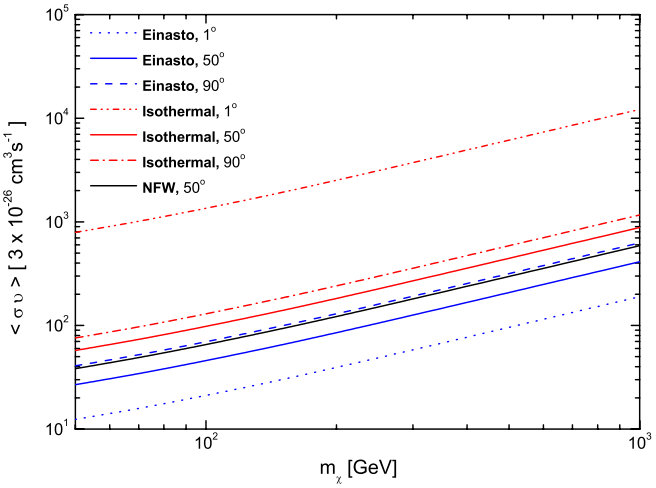

FIG. 4 (color online). The expected DeepCore sensitivities corresponding to different $\psi_{\max}$ for Einasto [31,32], Isothermal [34] and NFW [30] DM density profiles. We note that DeepCore sensitivities with $\psi_{\max} = 50°$ are denoted by solid lines, which, from top to bottom, correspond to sensitivities obtained by taking Isothermal, NFW, and Einasto DM density profiles, respectively.

distribution of the isothermal profile maintains flat for a much longer distance from the GC as compared to the cusped profile. However, as $\psi_{\max}$ increases further, the DeepCore sensitivity to the DM annihilation cross section becomes poorer even for the isothermal profile since the factor $J_2(\Delta\Omega)\Delta\Omega$ is proportional to the square of DM density. Finally, DeepCore sensitivities to the DM annihilation cross section with the isothermal profile are poorer than those with cusped profiles for the same $\psi_{\max}$. This results from the fact that DM densities of cusped profiles around GC are much larger than that of the isothermal profile in the same region.

Having discussed the effect of DM density profiles on the derived DeepCore sensitivities, we present in Fig. 5 the comparison of DeepCore sensitivities to $\langle\sigma(\chi\chi \to \mu^+\mu^-)v\rangle$ obtained by measuring cascade events and track events, respectively. We note that the NFW profile is adopted for results in this figure as well as results presented in the remaining figures of this article. We point out that ν_μ is the dominant flavor of atmospheric neutrinos above few tens of giga-electron volts and the neutrino-nucleon cross sections are almost the same for all flavors. Therefore, comparing with the result of track events, the signal to background ratio is enhanced in cascade events because ν_μ only produces the cascade events through the neutral-current interaction, which is lower in cross section than that of charged-current interaction. Hence cascade events in general provide better sensitivities to DM annihilation cross section than those provided by track events. We like to point out that the comparison between cascade and track events in Fig. 5 is based upon the current angular resolution of the IceCube detector. If the angular resolution for cascade events is improved in the future, the advantage of measuring cascade events would be even more significant as one can see from Fig. 3.

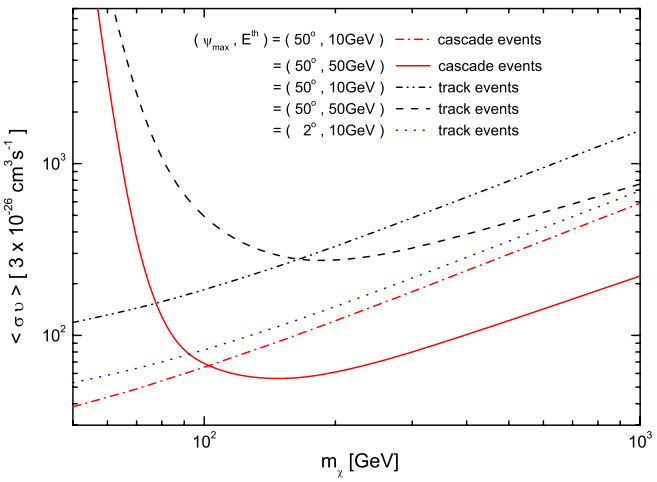

FIG. 5 (color online). The required DM annihilation cross section $(\chi\chi \to \mu^+\mu^-)$ as a function of m_χ such that the neutrino signature from DM annihilations can be detected at the 2σ significance in five years for track and cascade events.

It is interesting and essential to compare our results with constraints obtained from gamma-ray astronomy and cosmology. Fermi-LAT [56] is a pair-conversion telescope that explores the gamma-ray sky in the 20 MeV to 300 GeV range with unprecedented sensitivity. In a recent work, the Fermi-LAT Collaboration derives constraints on WIMP annihilation or decay into various final states, which produce a continuous photon spectrum [19]. These constraints are based upon the measured inclusive photon intensity spectrum from 4.8 to 264 GeV obtained from two years of Fermi-LAT data over the region $|b| > 10°$ plus a $20° \times 20°$ square region centered at GC with point sources removed. In Fig. 6, the dotted line is the cross section upper limit on the DM annihilation channel $\chi\chi \to \mu^+\mu^-$ from the diffuse gamma-ray spectrum with the NFW profile. It is taken from Ref. [19] with a rescaling factor $(4/3)^2$ applied since we have adopted a local density of $\rho_\odot = 0.3\ \mathrm{GeV/cm^3}$ while Fermi-LAT analysis uses $\rho_\odot = 0.4\ \mathrm{GeV/cm^3}$. Our expected 2σ sensitivities on the $\chi\chi \to \mu^+\mu^-$ annihilation cross section by the DeepCore detector with $\psi_{\max} = 50°$ and $\psi_{\max} = 10°$ are plotted for comparison. We can see that our expected 2σ sensitivity with $\psi_{\max} = 50°$ is slightly stronger than this Fermi-LAT constraint, even if we calculate the sensitivity with $V_{\mathrm{casc}}(E)$ given by Ref. [53]. Furthermore, the expected 2σ sensitivity with $\psi_{\max} = 10°$ in the DeepCore detector is almost an order of magnitude stronger than this Fermi-LAT constraint for small m_χ.

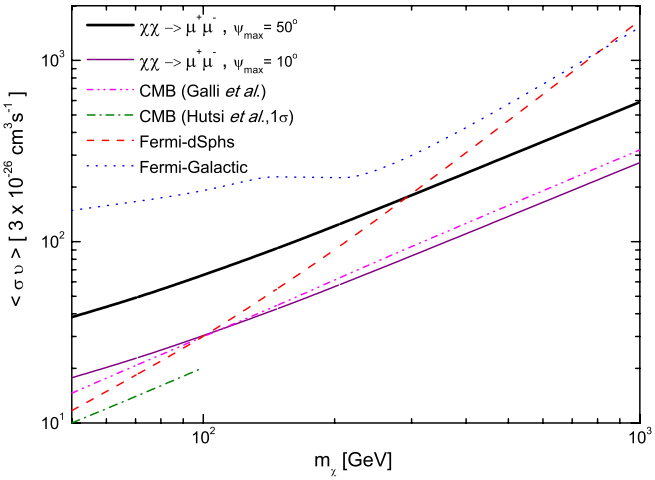

FIG. 6 (color online). Cross section limits on DM annihilation channel $\chi\chi \to \mu^+\mu^-$. The dot-dashed line is the 1σ upper bound on annihilation cross section for low-mass WIMP [22] obtained by WMAP7 data. The dot-dot-dashed line is the CMB constraint obtained by using WMAP7 + ACT data at 95% C.L. [23]. The dashed line is the dSphs constraint at 95% C.L. [20]. The dotted line is the constraint due to Fermi-LAT observations on the region $|b| > 10°$ plus a $20° \times 20°$ square region centered at GC, assuming the NFW profile [19]. The thick and thin solid lines are the expected 2σ sensitivities of the DeepCore detector with $(E_{\mathrm{sh}}^{\mathrm{th}}, \psi_{\max}) = (10\ \mathrm{GeV}, 50°)$ and $(E_{\mathrm{sh}}^{\mathrm{th}}, \psi_{\max}) = (10\ \mathrm{GeV}, 10°)$, respectively.

Constraints on the DM annihilation cross section were also obtained from cosmology and gamma-ray observations on dwarf spheroidal satellite galaxies (dSphs) of the Milky Way. Energy injection from DM annihilation at redshift $100 \lesssim z \lesssim 1000$ affects the CMB anisotropy. This is because the injected energy can ionize the thermal gas and modify the standard recombination history of the Universe. The updated CMB constraints on DM annihilation cross sections are derived in Refs. [22,23], where the former work is based on the recent WMAP 7-year data [24] while the latter one combines WMAP 7-year and ACT 2008 [25] data. We present the above two CMB constraints on the $\chi\chi \to \mu^+\mu^-$ annihilation cross section in Fig. 6. One can see that the thick solid line is higher than the dot-dot-dashed line (95% C.L.) by roughly a factor of 2. Thus the expected sensitivity of the IceCube DeepCore detector with $\psi_{\max} = 50°$ is slightly weaker than the CMB constraint. However, the DeepCore sensitivity is comparable to the CMB constraint with $\psi_{\max} = 10°$. It should be noted that the DM annihilation cross section could be velocity dependent. Hence, a model dependent extrapolation on the DM annihilation cross section might be required to compare the constraint on $\langle\sigma v\rangle$ at redshift $100 \lesssim z \lesssim 1000$ to that at the present day universe [57].

Dwarf spheroidal satellite galaxies of the Milky Way are DM-dominated systems that do not have active star formation or detected gas content [58,59]. Satellite galaxies are among the best targets to search for DM signals in gamma rays because of a small background from astrophysical sources and a favorable signal-to-noise ratio. In Ref. [20], the Fermi-LAT Collaboration derives upper limits on DM annihilation cross sections by applying a joint likelihood analysis to 24 months of data from 10 satellite galaxies with uncertainties on the dark matter distributions in the satellite galaxies taken into account. We present the dSphs constraint on the $\chi\chi \to \mu^+\mu^-$ annihilation cross section at 95% C.L. in Fig. 6. For $m_\chi > 300$ GeV, the expected DeepCore sensitivity curves are below that set by the dSphs constraint for both $\psi_{\max} = 50°$ and $\psi_{\max} = 10°$. For $m_\chi < 300$ GeV, the dSphs constraint is comparable to the expected DeepCore sensitivity with $\psi_{\max} = 10°$. Thus it is stronger than the expected DeepCore sensitivity with $\psi_{\max} = 50°$ in this DM mass range.

We also present Fermi-LAT's dSphs constraint and Galactic gamma-ray constraint on the $\chi\chi \to b\bar{b}$ annihilation cross section in Fig. 7. By comparing Figs. 6 and 7, we note that Fermi-LAT data give a more stringent constraint on the $\chi\chi \to b\bar{b}$ mode than its constraint on the $\chi\chi \to \mu^+\mu^-$ mode. This is in contrast to the DeepCore case, as one can see from Fig. 2. While the neutrino spectrum through $\chi\chi \to \mu^+\mu^-$ is harder than that through $\chi\chi \to b\bar{b}$, the gamma-ray spectra through the above annihilations behave differently. The gamma-ray spectrum from $\chi\chi \to b\bar{b}$ dominates over that from $\chi\chi \to \mu^+\mu^-$ for most of the range of $x = E_\gamma/m_\chi$ [60]. The expected 2σ sensitivity on

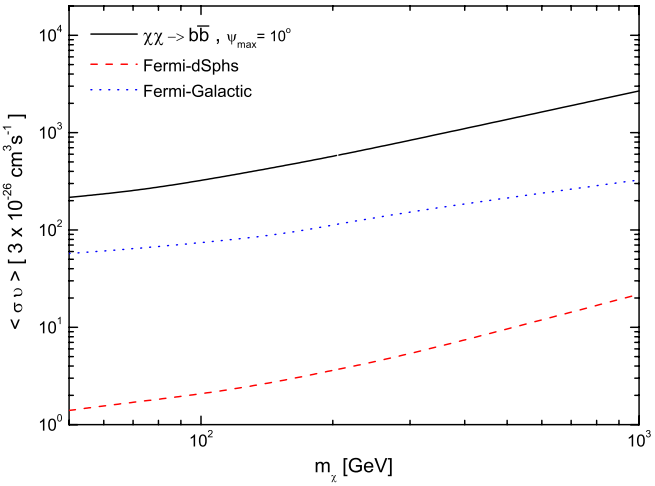

FIG. 7 (color online). Cross section limits on the DM annihilation channel $\chi\chi \to b\bar{b}$. The dashed line is the dSphs constraint at 95% C.L. [20]. The dotted line is the constraint due to Fermi-LAT observations for the region $|b| > 10°$ plus a $20° \times 20°$ square region centered at the GC, assuming the NFW profile [19]. The solid line is the expected 2σ sensitivity by the DeepCore detector with $E_{\rm sh}^{\rm th} = 10$ GeV and $\psi_{\max} = 10°$, which is weaker than both Fermi-LAT constraints. The DeepCore sensitivity with $\psi_{\max} = 50°$ is not shown since it is even less competitive.

the $\chi\chi \to b\bar{b}$ channel by the DeepCore detector with $\psi_{\max} = 10°$ is also shown in Fig. 7. One can see that the expected DeepCore sensitivity on this channel is weaker than all existing constraints presented here.

In addition to studying DeepCore sensitivities on DM annihilation channels, we also study sensitivities on the DM decay time for $\chi \to b\bar{b}$, $\tau^+\tau^-$, $\mu^+\mu^-$, and $\nu\bar{\nu}$ channels. Figure 8 shows the required DM decay time for reaching 2σ detection significance in five years on cascade events from each channel with the threshold energy $E_{\rm sh}^{\rm th} = 10$ GeV and a cone half-angle $\psi_{\max} = 50°$. Nondetection of such a signature would then exclude the parameter region below the curve at the 2σ level. We shall see later that the DeepCore sensitivity to DM decay time is not improved by considering $\psi_{\max}$ smaller than 50°. Comparing various DM decay modes, one can see that the $\chi \to \nu\bar{\nu}$ channel requires the lowest decay rate (longest decay time) to avoid a 2σ detection significance in five years of DeepCore data taking. We note that the energy-dependent effective volume $V_{\rm casc}(E)$ [53] downgrades the sensitivity to $\chi \to \nu\bar{\nu}$ decay time by roughly a factor of 1.5 at $m_\chi = 30$ GeV, which corresponds to $E_\nu = 15$ GeV. However, the sensitivity to $\chi \to \nu\bar{\nu}$ obtained with $V_{\rm casc}(E)$ is better than that presented in Fig. 8 for $m_\chi > 80$ GeV, which corresponds to $E_\nu > 40$ GeV. For the $\chi \to \mu^+\mu^-$ mode, the sensitivity at $m_\chi = 30$ GeV is lower by a factor of $\sqrt{3} \approx 1.7$ by applying $V_{\rm casc}(E)$, since such a m_χ corresponds to the lowest possible neutrino energy $E_\nu = 10$ GeV. However, $V_{\rm casc}(E)$ shall enhance the sensitivity

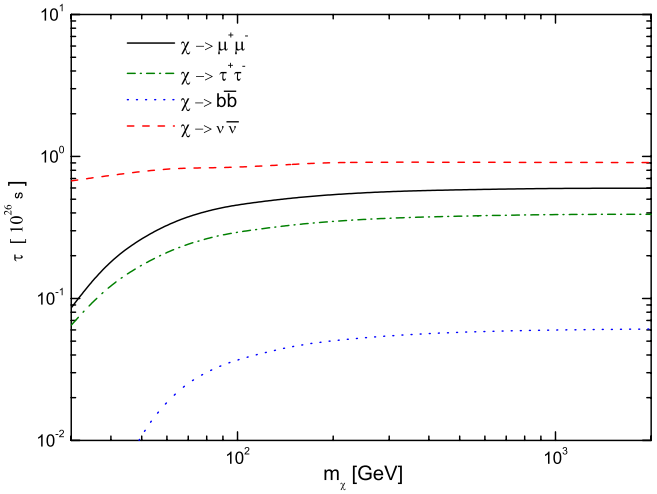

FIG. 8 (color online). The dotted line, the dot-dashed line, the solid line, and the dashed line are the expected DeepCore sensitivities to DM decay time through cascade events from decay channels $\chi \to b\bar{b}$, $\chi \to \tau^+\tau^-$, $\chi \to \mu^+\mu^-$, and $\chi \to \nu\bar{\nu}$, respectively.

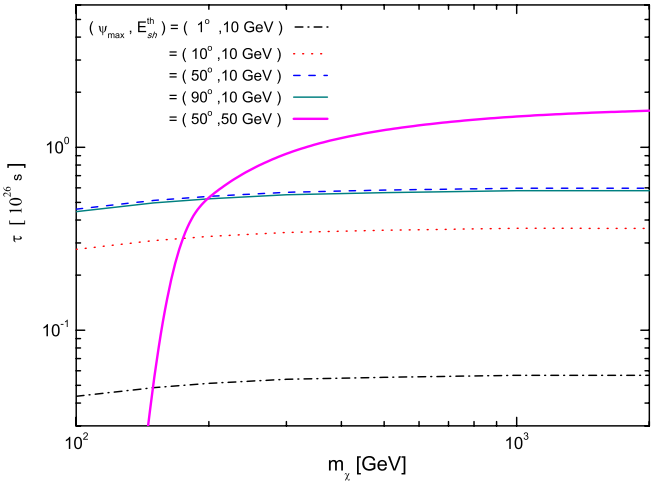

FIG. 9 (color online). The required DM decay time ($\chi \to \mu^+\mu^-$) as a function of m_χ such that the neutrino signature from DM decays can be detected at the 2σ significance in five years for cascade events. Results corresponding to different $\psi_{\max}$ are presented. For comparison, we also show the result with $E^{\rm th}_{\rm sh} = 50$ GeV and $\psi_{\max} = 50°$ [17]. We note that the thin solid line corresponds to $E^{\rm th}_{\rm sh} = 10$ GeV and $\psi_{\max} = 90°$ while the thick solid line corresponds to $E^{\rm th}_{\rm sh} = 50$ GeV and $\psi_{\max} = 50°$.

for $m_\chi > 240$ GeV, which corresponds to $E_\nu = 40$ GeV, assuming $E_\nu \simeq m_\chi/6$. The correction factor for $\chi \to \tau^+\tau^-$ is similar to that for $\chi \to \mu^+\mu^-$, while the hadronic mode $\chi \to b\bar{b}$ requires a different correction factor for the same m_χ. Once more, we do not address such a correction, as the DeepCore detector is relatively insensitive to $\chi \to b\bar{b}$.

Next, we show how the DeepCore sensitivity on DM decay time varies with the chosen cone half-angle and threshold energy. We use the $\chi \to \mu^+\mu^-$ channel to illustrate these effects. In Fig. 9, we present the required DM decay time ($\chi \to \mu^+\mu^-$) as a function of m_χ for reaching 2σ detection significance in five years for different cone half-angle $\psi_{\max}$. The sensitivity curve rises as $\psi_{\max}$ increases from 1° to 50°. As $\psi_{\max}$ increases in this cone half-angle range, the DM event rate increases faster than that of atmospheric background. However, the sensitivity is not further improved by increasing $\psi_{\max}$ from 50° to 90°. We also show the required DM decay time for a 2σ detection significance in five years with $E^{\rm th}_{\rm sh} = 50$ GeV and $\psi_{\max} = 50°$ for comparison. It has been pointed out in Ref. [17] that $\psi_{\max} = 50°$ gives rise to the highest sensitivity on DM decay time for $E^{\rm th}_{\rm sh} = 50$ GeV. We note that the sensitivity on DM decay time is improved by lowering $E^{\rm th}_{\rm sh}$ from 50 to 10 GeV for $m_\chi < 200$ GeV.

It is of interest to compare sensitivities on DM decay time given by cascade events and track events. In Fig. 10, one can see that cascade events provide better sensitivity on DM decay time than that given by track events for the same threshold energy $E^{\rm th}$ and $\psi_{\max}$. In the same figure we also show the sensitivity given by track events for $\psi_{\max} = 90°$. Such a $\psi_{\max}$ renders the best sensitivity for track events. However, this sensitivity is still poorer than those given by cascade events.

In Fig. 11, we present decay time lower limits for $\chi \to \mu^+\mu^-$ and $\chi \to b\bar{b}$ channels obtained from the diffuse gamma-ray spectrum for the region $|b| > 10°$ plus a $20° \times 20°$ square region centered at GC, assuming the NFW profile. They are taken from Ref. [19], with a rescaling factor of 3/4 applied since we have adopted a local density of $\rho_\odot = 0.3$ GeV/cm^3 while Fermi-LAT analysis uses $\rho_\odot = 0.4$ GeV/cm^3. In the same figure, we also show the expected 2σ sensitivities to $\chi \to \mu^+\mu^-$ and $\chi \to b\bar{b}$ decay time by the DeepCore detector with $\psi_{\max} = 50°$ for

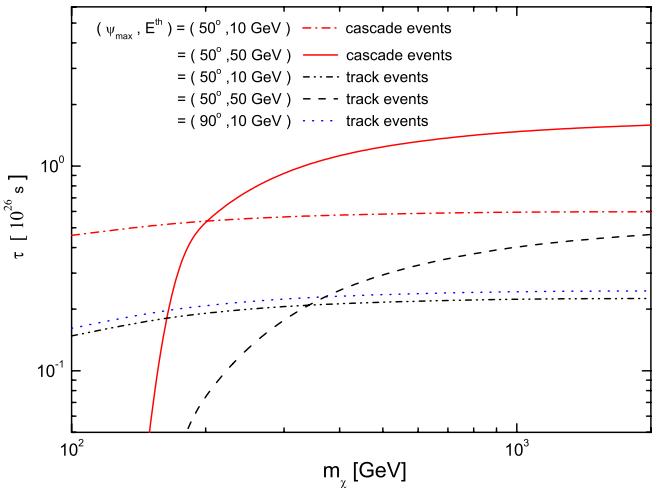

FIG. 10 (color online). The required DM decay time ($\chi \to \mu^+\mu^-$) as a function of m_χ such that the neutrino signature from DM decays can be detected at the 2σ significance in five years for track and cascade events.

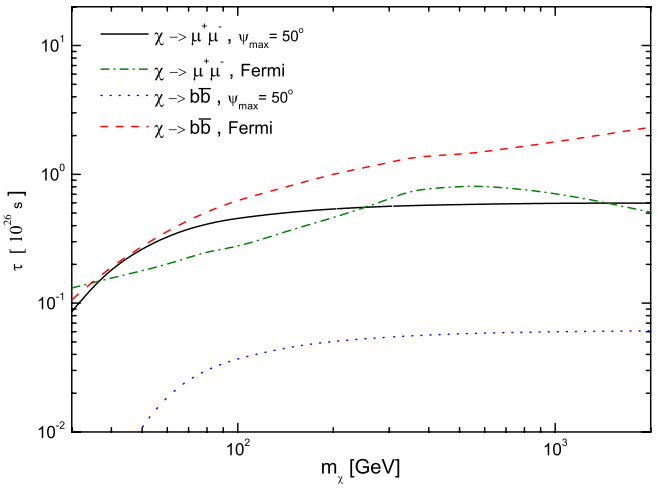

FIG. 11 (color online). The dot-dashed line and dashed line are the decay time constraints for $\chi \to \mu^+\mu^-$ and $\chi \to b\bar{b}$ channels due to Fermi observations for the region $|b| > 10°$ plus a $20° \times 20°$ at GC, assuming the NFW profile [19]. The solid line and dotted line are our expected 2σ sensitivities for $\chi \to \mu^+\mu^-$ and $\chi \to b\bar{b}$ channels with $E_{\rm sh}^{\rm th} = 10$ GeV and $\psi_{\rm max} = 50°$.

comparisons. For the DeepCore detector, the sensitivity to the $\chi \to \mu^+\mu^-$ decay time is better than that to the $\chi \to b\bar{b}$ decay time, since the neutrino spectrum in the former channel is harder than the one in the latter channel. On the other hand, the Fermi-LAT data in general gives a more stringent constraint on $\chi \to b\bar{b}$ decay time than its constraint on the decay time of $\chi \to \mu^+\mu^-$. This is because that the gamma-ray spectrum from the former channel dominates over the one from the latter channel for most of the range of $x = E_\gamma/m_\chi$, as the DM annihilation case. If DM decays predominantly into $\mu^+\mu^-$, one can see that the decay time sensitivity expected at DeepCore is comparable to the constraint given by Fermi-LAT data. This conclusion is not altered by adopting the energy-dependent effective volume $V_{\rm casc}(E)$ [53]. On the other hand, if DM decays predominantly to $b\bar{b}$, the expected DeepCore sensitivity is much poorer than the constraint from Fermi-LAT data.

V. DISCUSSIONS AND CONCLUSIONS

In this paper, we have evaluated sensitivities of the IceCube DeepCore detector to neutrino cascade events induced by DM annihilations and decays in the Galactic halo. We focus on the scenario of the small DM mass, and the threshold energy for the cascade events is taken to be 10 GeV. The event rate of background atmospheric neutrinos is calculated with $\nu_\mu \to \nu_\tau$ oscillations taken into account for neutrino energies less than 40 GeV. The signal event rate is calculated by taking the NFW profile for DM density distribution in the Galactic halo. Among all DM annihilation and decay channels, the annihilation mode $\chi\chi \to \nu\bar{\nu}$ and the decay mode $\chi \to \nu\bar{\nu}$ provide the best search sensitivity, while the search sensitivity provided by the annihilation mode $\chi\chi \to b\bar{b}$ and the decay mode $\chi \to b\bar{b}$ is the poorest.

It is important to compare the expected sensitivities of the DeepCore detector to the DM annihilation cross section and decay time with the existing constraints on the same quantities obtained by cosmology and Fermi-LAT gamma-ray observations. It is seen that the Fermi-LAT constraints on $\chi\chi \to b\bar{b}$ and $\chi \to b\bar{b}$ are much stronger than the expected DeepCore sensitivities to the same channels. Hence, if DM predominantly annihilates or decays into $b\bar{b}$, the DeepCore detector is not expected to observe the neutrino signature induced by DM in the Galactic halo. For leptonic final states, one can see from Fig. 6 that the expected DeepCore sensitivity to the $\chi\chi \to \mu^+\mu^-$ annihilation cross section is stronger than the Fermi-LAT constraint on the same channel based upon gamma-ray data from the Galactic halo. However, the former sensitivity with the current angular resolution of cascade events is slightly weaker than both the dSphs constraint and the constraint obtained from WMAP and ACT results on CMB anisotropy. On the other hand, the DeepCore sensitivity can be improved with an improved angular resolution for cascade events. In Fig. 11, we also see that the expected DeepCore sensitivity to $\chi \to \mu^+\mu^-$ decay time is comparable to the Fermi-LAT constraint based upon gamma-ray data from the Galactic halo. From the above comparisons, there remain slight possibilities to observe the DM-induced neutrino signature from the Galactic halo provided DM annihilates or decays predominantly into leptons.

It should be noted that Fermi-LAT and CMB data does not directly set limits on $\chi\chi \to \nu\bar{\nu}$ or $\chi \to \nu\bar{\nu}$ modes with monochromatic neutrinos. There exist models [61,62] in which $\chi\chi \to \nu\bar{\nu}$ and $\chi \to \nu\bar{\nu}$ are dominant annihilation and decay modes, respectively. In the annihilation case [61], for example, the DM candidate can be the lightest right-handed (RH) sneutrino in a $U(1)_{B-L}$ extension of the minimal supersymmetric standard model. RH sneutrinos annihilate into a pair of RH neutrinos. Each of these RH neutrinos then decays into an ordinary left-handed neutrino and a neutral Higgs boson while the decay of the RH neutrino into charged final states $l^\pm h^\mp$ is typically forbidden in such a model. In the case that the mass difference between RH sneutrinos and RH neutrinos is small, RH neutrinos are produced nonrelativistically by DM annihilations. Hence left-handed neutrinos produced by the decays of RH neutrinos are approximately monochromatic with an energy around half of the DM mass. Therefore the sensitivity of IceCube DeepCore to this type of models can be read off from the $\chi\chi \to \nu\bar{\nu}$ curve in Fig. 2 with the shift $(\langle\sigma v\rangle, m_\chi) \to (\langle\sigma v\rangle, 2m_\chi)$.

Before closing, we comment on the detection of the neutrino signature induced by DM in the Galactic halo with neutrino telescopes in the Northern Hemisphere. Generally a neutrino telescope in such a location has advantages in detecting tracklike neutrino events. First,

the telescope's effective volume for upward going track events is enhanced by the muon range. This effect is particularly significant for energetic track events originated from high-energy muon neutrinos. Second, a neutrino telescope in the Northern Hemisphere naturally suppresses the atmospheric muon background while IceCube needs to use optical modules located at the outer region for vetoing the same background [63]. Following these arguments, it is interesting to see if a detector array in the Northern Hemisphere with the size of the DeepCore detector has a significantly better sensitivity than the current DeepCore detector surrounded by IceCube strings. Since the latter also has a good veto capability, the former can gain only in the effective volume expected to be enhanced by the muon range. We note that the DeepCore array aims at detecting neutrinos in the energy range $10 \leq E_\nu/\mathrm{GeV} \leq 100$. Muons induced by muon neutrinos in this energy range only travel around 50 m for $E_\mu = 10$ GeV and 400 m for $E_\mu = 100$ GeV. This does not significantly enhance the detector's effective volume in most cases since the height of the DeepCore detector is already around 350 m. Therefore, given the existence of the IceCube detector augmented by DeepCore in the South Pole, it is clear that neutrino telescopes in the Northern Hemisphere only have advantages in detecting the neutrino signature from heavier DM. In this regard, the acceptance for track events in KM3NeT as a function of neutrino energy has been estimated [64]. With this acceptance, we also calculate the sensitivity of KM3NeT to the DM annihilation cross section $\langle\sigma(\chi\chi \to \mu^+\mu^-)v\rangle$ in the Galactic halo. For $\psi_{\mathrm{max}} = 10^\circ$ and $m_\chi = 200$ GeV, the KM3NeT 2σ sensitivity to $\langle\sigma(\chi\chi \to \mu^+\mu^-)v\rangle$ in 5 years is comparable to the CMB constraint on this channel [23]. However, for $m_\chi = 1$ TeV, the CMB constraint gives $\langle\sigma(\chi\chi \to \mu^+\mu^-)v\rangle$ no greater than 10^{-23} cm^3 s^{-1}, whereas the KM3NeT 2σ sensitivity on the same annihilation channel can reach to 1.5×10^{-24} cm^3 s^{-1} in 5 years.

In conclusion, we have made detailed comparisons between IceCube DeepCore sensitivities and other existing constraints on various DM annihilation and decay channels. The prospect for the DeepCore detector to observe the neutrino signature induced by DM in the Galactic halo has been discussed. We have also mentioned the expected performance of KM3NeT on this observation.

ACKNOWLEDGMENTS

We thank Y.-H. Lin for useful discussions and C. Rott for bringing Ref. [53] to our attention. F. F. L. is supported by a grant from Research and Development Office, National Chiao-Tung University, G. L. L. is supported by National Science Council of Taiwan under Grant No. 99-2112-M-009-005-MY3, and Y. S. T. is funded in part by the Welcome Program of the Foundation for Polish Science.

[1] G. Jungman, M. Kamionkowski, and K. Griest, Phys. Rep. **267**, 195 (1996); L. Bergstrom, Rep. Prog. Phys. **63**, 793 (2000).
[2] G. Bertone, D. Hooper, and J. Silk, Phys. Rep. **405**, 279 (2005).
[3] A. Achterberg *et al.* (IceCube Collaboration), Astropart. Phys. **26**, 155 (2006).
[4] R. Abbasi *et al.* (IceCube Collaboration), Phys. Rev. D **84**, 022004 (2011).
[5] R. Abbasi *et al.* (IceCube Collaboration), arXiv:1111.2738.
[6] R. Abbasi *et al.* (IceCube Collaboration), Phys. Rev. D **84**, 082001 (2011).
[7] I. F. M. Albuquerque, L. J. B. e Silva, and C. P. de los Heros, Phys. Rev. D **85**, 123539 (2012).
[8] O. Adriani *et al.* (PAMELA Collaboration), Phys. Rev. Lett. **106**, 201101 (2011).
[9] M. Ackermann *et al.* (Fermi-LAT Collaboration), Phys. Rev. D **82**, 092004 (2010).
[10] E. Resconi (IceCube Collaboration), Nucl. Instrum. Methods Phys. Res., Sect. A **602**, 7 (2009).
[11] C. Wiebusch, for the IceCube Collaboration, arXiv:0907.2263.
[12] T. DeYoung (IceCube Collaboration), Nucl. Instrum Methods Phys. Res., Sect. A **692**, 180 (2012).
[13] D. Spolyar, M. R. Buckley, K. Freese, D. Hooper, and H. Murayama, arXiv:0905.4764.
[14] M. R. Buckley, D. Spolyar, K. Freese, D. Hooper, and H. Murayama, Phys. Rev. D **81**, 016006 (2010).
[15] S. K. Mandal, M. R. Buckley, K. Freese, D. Spolyar, and H. Murayama, Phys. Rev. D **81**, 043508 (2010).
[16] L. Covi, M. Grefe, A. Ibarra, and D. Tran, J. Cosmol. Astropart. Phys. 04 (2010) 017.
[17] A. E. Erkoca, M. H. Reno, and I. Sarcevic, Phys. Rev. D **82**, 113006 (2010).
[18] F. F. Lee and G. L. Lin, Phys. Rev. D **85**, 023529 (2012).
[19] M. Ackermann *et al.* (Fermi-LAT Collaboration), Phys. Rev. D **86**, 022002 (2012).
[20] M. Ackermann *et al.* (Fermi-LAT Collaboration), Phys. Rev. Lett. **107**, 241302 (2011).
[21] M. Cirelli, P. Panci, and P. D. Serpico, Nucl. Phys. **B840**, 284 (2010).
[22] G. Hutsi, J. Chluba, A. Hektor, and M. Raidal, Astron. Astrophys. **535**, A26 (2011).
[23] S. Galli, F. Iocco, G. Bertone, and A. Melchiorri, Phys. Rev. D **84**, 027302 (2011).
[24] E. Komatsu *et al.*, Astrophys. J. Suppl. Ser. **192**, 18 (2011).
[25] J. W. Fowler *et al.*, Astrophys. J. **722**, 1148 (2010).

[26] J. Hisano, M. Kawasaki, K. Kohri, and K. Nakayama, Phys. Rev. D **79**, 043516 (2009).

[27] A. E. Erkoca, G. Gelmini, M. H. Reno, and I. Sarcevic, Phys. Rev. D **81**, 096007 (2010).

[28] A. Sommerfeld, Ann. Phys. (Leipzig) **403**, 257 (1931); J. Hisano, S. Matsumoto, and M. M. Nojiri, Phys. Rev. Lett. **92**, 031303 (2004); J. M. Russell, S. M. West, D. Cumberbatch, and D. Hooper, J. High Energy Phys. 07 (2008) 058; N. Arkani-Hamed, D. P. Finkbeiner, T. R. Slatyer, and N. Weiner, Phys. Rev. D **79**, 015014 (2009); I. Cholis, G. Dobler, D. P. Finkbeiner, L. Goodenough, and N. Weiner, Phys. Rev. D **80**, 123518 (2009); J. M. Russell and S. M. West, Phys. Lett. B **676**, 133 (2009); S. M. Koushiappas and M. Kamionkowski, Phys. Rev. Lett. **103**, 121301 (2009); M. Kamionkowski, S. M. Koushiappas, and M. Kuhlen, Phys. Rev. D **81**, 043532 (2010); M. Lindner, A. Merle, and V. Niro, Phys. Rev. D **82**, 123529 (2010); D. Suematsu, T. Toma, and T. Yoshida, Phys. Rev. D **82**, 013012 (2010); S. Hannestad and T. Tram, J. Cosmol. Astropart. Phys. 01 (2011) 016; J. L. Feng, M. Kaplinghat, and H.-B. Yu, Phys. Rev. D **82**, 083525 (2010); C. Arina, F.-X. Josse-Michaux, and N. Sahu, Phys. Lett. B **691**, 219 (2010).

[29] P. Gondolo, J. Edsjo, P. Ullio, L. Bergstrom, M. Schelke, and E. A. Baltz, J. Cosmol. Astropart. Phys. 07 (2004) 008.

[30] J. F. Navarro, C. S. Frenk, and S. D. M. White, Astrophys. J. **462**, 563 (1996).

[31] D. Merritt, A. W. Graham, B. Moore, J. Diemand, and B. Terzić, Astron. J. **132**, 2685 (2006).

[32] J. F. Navarro *et al.*, arXiv:0810.1522.

[33] J. Diemand, M. Kuhlen, P. Madau, M. Zemp, B. Moore, D. Potter, and J. Stadel, Nature (London) **454**, 735 (2008).

[34] J. N. Bahcall and R. M. Soneira, Astrophys. J. Suppl. Ser. **44**, 73 (1980).

[35] J. G. Learned and S. Pakvasa, Astropart. Phys. **3**, 267 (1995).

[36] H. Athar, M. Jezabek, and O. Yasuda, Phys. Rev. D **62**, 103007 (2000); L. Bento, P. Keranen, and J. Maalampi, Phys. Lett. B **476**, 205 (2000).

[37] See also K. C. Lai, G. L. Lin, and T. C. Liu, Phys. Rev. D **80**, 103005 (2009).

[38] K. Abe *et al.* (T2K Collaboration), Phys. Rev. Lett. **107**, 041801 (2011).

[39] Y. Abe *et al.* (DOUBLE-CHOOZ Collaboration), Phys. Rev. Lett. **108**, 131801 (2012).

[40] F. P. An *et al.* (DAYA-BAY Collaboration), Phys. Rev. Lett. **108**, 171803 (2012).

[41] J. K. Ahn *et al.* (RENO Collaboration), Phys. Rev. Lett. **108**, 191802 (2012).

[42] G. L. Fogli, E. Lisi, A. Marrone, D. Montanino, A. Palazzo, and A. M. Rotunno, Phys. Rev. D **86**, 013012 (2012).

[43] T. K. Gaisser, Astropart. Phys. **16**, 285 (2002).

[44] F. F. Lee and G. L. Lin, Astropart. Phys. **25**, 64 (2006).

[45] T. K. Gaisser and M. Honda, Annu. Rev. Nucl. Part. Sci. **52**, 153 (2002).

[46] M. Honda, T. Kajita, K. Kasahara, and S. Midorikawa, Phys. Rev. D **70**, 043008 (2004).

[47] P. Lipari, Astropart. Phys. **1**, 195 (1993).

[48] M. Honda, T. Kajita, K. Kasahara, S. Midorikawa, and T. Sanuki, Phys. Rev. D **75**, 043006 (2007).

[49] R. Abbasi *et al.*, Astropart. Phys. **34**, 48 (2010).

[50] T. K. Gaisser, *Cosmic Rays and Particle Physics* (Cambridge University Press, Cambridge, England, 1992).

[51] A. B. McDonald, C. Spiering, S. Schonert, E. T. Kearns, and T. Kajita, Rev. Sci. Instrum. **75**, 293 (2004).

[52] R. Gandhi, C. Quigg, M. H. Reno, and I. Sarcevic, Astropart. Phys. **5**, 81 (1996); Phys. Rev. D **58**, 093009 (1998).

[53] R. Abbasi *et al.* (IceCube Collaboration), Astropart. Phys. **35**, 615 (2012).

[54] E. Middell, J. McCartin, and M. D'Agostino, in *Proceedings of the 31st ICRC, Lodz 2009.*

[55] R. Auer, Nucl. Instrum. Methods Phys. Res., Sect. A **602**, 84 (2009).

[56] W. B. Atwood *et al.* (Fermi-LAT Collaboration), Astrophys. J. **697**, 1071 (2009).

[57] For discussions on this issue, see, for example, J. Hisano, M. Kawasaki, K. Kohri, T. Moroi, K. Nakayama, and T. Sekiguchi, Phys. Rev. D **83**, 123511 (2011).

[58] M. Mateo, Annu. Rev. Astron. Astrophys. **36**, 435 (1998).

[59] J. Grcevich and M. E. Putman, Astrophys. J. **696**, 385 (2009).

[60] The spectral shapes of gamma ray and neutrinos from DM annihilations are summarized in M. Cirelli, G. Corcella, A. Hektor, G. Hütsi, M. Kadastik, P. Panci, M. Raidal, F. Sala, and A. Strumia, J. Cosmol. Astropart. Phys. 03 (2011) 051, where original references are listed.

[61] R. Allahverdi, S. Bornhauser, B. Dutta, and K. Richardson-McDaniel, Phys. Rev. D **80**, 055026 (2009).

[62] A. Falkowski, J. Juknevich, and J. Shelton, arXiv:0908.1790.

[63] R. Abbasi *et al.* (IceCube Collaboration), arXiv:1210.3557.

[64] KM3NeT Collaboration, Technical Design Report, http://www.km3net.org/TDR/TDRKM3NeT.pdf.